Intrinsic electric fields and Raman spectra of III-V nitride wurtzite semiconductor heterostructures

D. Coffey and N. Bock
Department of Physics, State University of New York, Buffalo, New York 14260
(Received 6 August 1998)

The analysis of Raman data on semiconductor nitride heterostructures is complicated by large intrinsic electric fields. This issue is analyzed here by calculating the Raman signal for quantum wells made from wurtzite AlN-GaN. The signature of the confined phonon modes in GaN quantum wells is calculated and found to be strongly effected by the intrinsic electric fields due to lattice mismatch and the piezoelectric character of the materials. This calculation suggests that the effects of electric fields on the electronic states in III-V nitride heterostructures should be taken into account in the analysis of Raman spectra in these materials and that the application of realizable external electric fields would be a useful probe of these materials.
[S0163-1829(99)02508-4]

I. INTRODUCTION

Raman spectroscopy can be used to probe the nature of the carrier-phonon interaction in semiconductor heterostructures and can lead to information on carrier relaxation rates important in transport properties.[1] This interaction can be characterized in terms of deformation-potential contributions and the contribution from the Fröhlich interaction. Here we concentrate on the Fröhlich contribution and in particular on the effect of the internal electric fields in wurtzite III-V semiconductor heterostructures due to spontaneous polarization and their piezoelectric character[2–4] on the Raman spectrum of heterostructure phonons. The calculations require a model for both the electronic and phonon properties.

The electronic properties are treated in the envelope approximation with the values of the band effective masses taken from fits to recent band-structure calculations and the values of band offsets are taken from experiment. In systems with wurtzite symmetry the absence of a center of inversion leads to spontaneous polarization and any lattice mismatch results in strong electric fields because of the piezoelectric properties of these materials. The strain and electric fields due to lattice mismatch in heterostructures are reduced by defect formation to different extents in different samples. Since there is as yet no detailed comparison with experiment, different strengths of electric field will be considered here to illustrate the effect of these fields on the Raman signal.

Optical phonon frequencies were first measured on wurtzite crystals, BeO, ZnO, ZnS, and CdS, using Raman spectroscopy by Porto and collaborators,[5] and the symmetry allowed phonon modes were detected. Similar measurements have been performed on wurtzite GaN and AlN,[6–8] but only results for the $A_1(\mathrm{LO})$ and one of the E_2 modes in InN have been published so far.[9] Given measurements of the bulk optical phonon spectrum, the phonon dispersion for the whole zone can de determined using a valence-Coulomb force field model for the lattice potential energy[10,11] where the parameters of the model are determined by fits to the optical phonon frequencies. The values of the parameters for the bulk materials can be used to construct models for the phonon modes of heterostructures.[12,13] In the present calculation the phonon modes of an AlN-GaN heterostructure are modeled by confining the bulk modes to the well and barrier materials. This is motivated by the large differences in frequencies between modes of the same symmetry in these materials. The low symmetry of the bulk materials is not significantly affected by growth of heterostructures along the c axis except for the introduction of a set of slab and guide modes for each phonon symmetry. Here we identify the confined modes associated with the bulk GaN $A_1(\mathrm{LO})$ phonon as the mode most likely to give a signature of confined phonons. The slab modes are found here to have a very strong contribution to the Raman spectrum. Interface modes also are present for heterostructures and have been detected experimentally.[14] However, in the interests of simplicity these modes have not been included for the narrow GaN wells considered here.

The Raman signal was calculated for an AlN-GaN-AlN quantum well. The calculations concentrated on the signature of the confined phonon modes in GaN quantum wells where the intrinsic electric fields due to lattice mismatch and the piezoelectric character of the materials are shown to lead to a strong influence on the Raman signal. This arises from the breakdown of parity symmetry for the hole and electron wave functions. The influence of external electric fields on resonant Raman spectra has previously been examined for GaAs/AlAs heterostructures[15–17] where large external fields lead to similar effects. In GaN/AlN quantum wells the effects of intrinsic fields with values comparable to external fields discussed by previous authors are found to be larger because of the different values of the parameters entering into the envelope approximation for the electronic wave functions. The outline of the paper is as follows. The model for the electronic wave functions is discussed in Sec. II and that for the phonon modes is discussed in Sec. III. The Raman spectrum in the presence of strong electric fields in GaN quantum wells is presented in Sec. IV. and finally conclusions are given in the last section.

II. ELECTRONIC WAVE FUNCTIONS

The C_{6v} symmetry of the wurtzite crystal splits the valence band into three, one of which has Γ_9 symmetry and

two others with Γ_7 symmetry. The valence-band edges of the heavy-hole (hh) and light-hole (lh) bands are separated by about 10 meV while the split-off band has an energy gap to the conduction band which is bigger than their energy gaps by about 40 meV.

Assuming parabolic bands, for the conduction and valence bands, effective masses are required. There are estimates for the electron effective mass from the point defect studies of Tansley and Egan.[18] These values are $0.12m_e$(InN), $0.20m_e$(GaN), and $0.33m_e$(AlN), which are in good agreement with estimates based on fitting to first-principles band-structure calculations.[19–21] In the present calculation we have considered GaN($E_{\rm gap}=3.4$ eV) quantum wells and AlN($E_{\rm gap}=6.2$ eV) as the barrier material. The large band offsets between well and barrier material ensure that the wave functions associated with the lowest energy confined subbands are strongly localized in the wells.

Growing GaN quantum wells pseudomorphically on AlN material introduces strain because of the lattice mismatch. In these piezoelectric materials this leads to an internal electric field along the direction of growth. The effect of the electric fields is to remove parity as a good quantum number for the electron and hole states. The effect of these electric fields on valence-band discontinuities has recently been discussed by Martin *et al.*,[22] who also gave an estimate for the strain induced electric fields for GaN grown on AlN of $\sim 5\times 10^6$ V cm^{-1}(50 meV Å^{-1}). The observed electric field magnitude is considerably less than this due to the relaxation of strain by defect formation which occurs beyond a critical thickness of the well, which is estimated to ~ 30 Å.[23] The resultant defects lead to impurity scattering of the phonon and electronic states which can be modeled by an imaginary term in the energy denominators describing intermediate states. In the present calculations we consider different strengths of internal electric field which are not determined by the extent of lattice mismatch. The difference between these values and those given by lattice mismatch and the piezoelectric constants of the materials can be thought of as arising from the reduction in strain due to defect formation.

The excitonic states confined to the quantum well are calculated allowing for both finite well depths and the possibility of an internal electric field coming from strain. The Hamiltonian has three components: H_z^e and H_z^h, Hamiltonians for the subbands associated with the conduction band and the different hole bands, and $H_{\rm 2D}^{eh}$, the Hamiltonian for the two-dimensional hydrogen atom. The terms in the Hamiltonian are

$$H_z^e=\left(\frac{-\hbar^2}{2m_c^{\parallel}(z_e)}\frac{d^2}{dz_e^2}+V_e(z_e)-F(z_e)\right)\phi_{n_e}(z_e)=e_{n_e}\phi_{n_e}(z_e),$$

$$H_z^h=\left(\frac{-\hbar^2}{2m_h^{\parallel}(z_h)}\frac{d^2}{dz_h^2}+V_h(z_h)+F(z_h)\right)\psi_{n_h}(z_h)=e_{n_h}\psi_{n_h}(z_h), \tag{1}$$

$$H_{\rm 2D}^{eh}=\left(\frac{-\hbar^2}{2\mu}\frac{1}{\rho}\frac{\partial}{\partial\rho}\left(\rho\frac{\partial}{\partial\rho}\right)-\frac{e^2}{\epsilon_0\rho}\right)\Lambda_{n_X}(\rho)=e_{n_X}\Lambda_{n_X}(\rho).$$

The $V_e(z_e)$ and $V_h(z_h)$ are the confining potentials determined from the band offsets and $F(z)=eE_0z$ inside the wells, $eE_0(w/2)$ for $z>w/2$, and $-eE_0(w/2)$ for $z<-w/2$, where E_0 is the electric field introduced by lattice mismatch and w is the width of the wells. For AlN-GaN-AlN quantum wells these are given values $V_v=0.7$ eV and $V_c=2.1$ eV from the work of Martin *et al.*[22]

TABLE I. Effective masses [from Kim *et al.* (Ref. 21)].

	$m_c^{\parallel}$	$m_c^{\perp}$	$m_{\rm hh}^{\parallel}$	$m_{\rm lh}^{\parallel}$	$m_{\rm split}^{\parallel}$	$m_{\rm hh}^{\perp}$	$m_{\rm lh}^{\perp}$	$m_{\rm split}^{\perp}$
AlN	0.35	0.35	3.68	3.68	0.25	6.33	0.25	3.68
GaN	0.19	0.23	1.10	1.10	0.15	1.65	0.15	1.10

As mentioned above, there are three valence bands, heavy-hole (hh), light-hole (lh), and split off (split), which are close in energy. Assuming a well width equal to 26 Å, or five GaN layers, and using the values of the effective masses in Table I, the subband energies in the absence of an electric field are at 0.207 eV, 0.806 eV, 1.653 eV for the conduction band, 0.042 eV, 0.170 eV, 0.369 eV, and 0.576 eV for the hh and lh bands, and 0.154 eV and 0.495 eV for the split band. The difference in the lowest subband energies for the lh and split bands ensures that the strong nonparabolicity of these bands seen in Fig. 2 of Ref. 21 does not occur until energies ~ 150 meV above the band edge determined by the lowest hh subband. Further, because $m_{\rm hh}^{\perp}>25m_{\rm lh}^{\perp}$, the density of states associated with motion in the plane transverse to the direction of growth for the lh band is much smaller than that of the hh band. Consequently the optical response is dominated by the hh band and the lh contribution can be dropped.

$\Lambda_{n_X}(\rho)$ are solutions of the effective two-dimensional hydrogen atom.[24] Using bulk parameters for GaN, the effective Bohr radius in the plane perpendicular to the c axis, $a_{\rm Bohr}$, is ~ 28 Å, which is comparable in size to the size of the wells considered in the calculation and the excitonic bound state energies are $e_{n_X}=-0.112$ eV$/(2n_X-1)^2$. The magnitudes of these energies will be reduced due to the quasi-three-dimensional nature of the wells.

For incident photon energies very close to or greater than $E_{\rm gap}$, the detailed structure of the excitonic states, including the nonparabolicity of the lh and split bands, will have a signature in the frequency dependence of the resonant Raman signal. However, in the present case photons with energies at $\sim 0.75E_{\rm gap}$ are considered so that an average over hole bands determines the optical response. Consequently in the calculations of the Raman spectrum only the conduction and hh subbands are included. It is the destruction of the even and odd parity of the states with respect to the center of the well by the intrinsic electric fields that is responsible for their strong effect on the Raman signal rather than the details of the excitonic states. This is taken into account in our approximation in which the effects of the lowest-energy four hh subbands are included.

In Figs. 1 and 2 the subband wave functions are plotted with $E_0=0$, $E_0=1$ meV Å^{-1}, and $E_0=10$ meV Å^{-1} for the $n_e=1$ and $n_{\rm hh}=1$ subbands. The changes in the wave functions seem to be modest especially for the electron states. However, the electric field ensures that the confined electronic states are no longer parity eigenstates, which has a

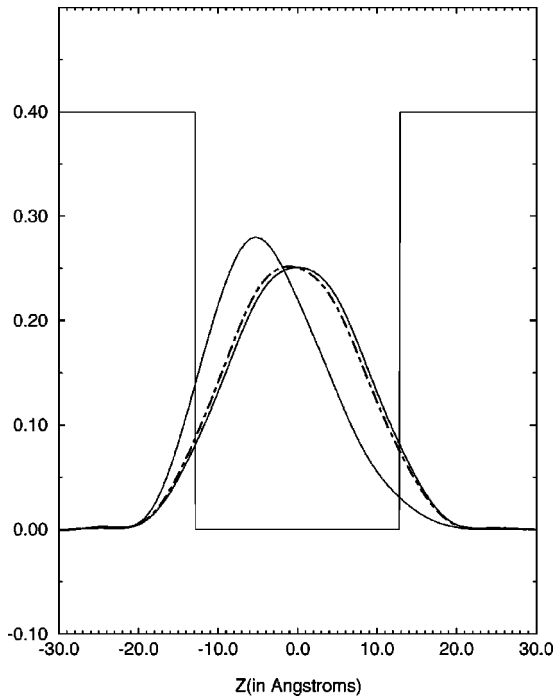

FIG. 1. Lowest confined electron subband in different electric fields, $E_0=0$ (solid line), $E_0=1.0$ meV Å^{-1} (100 kV cm^{-1}) (dot-dashed), and $E_0=10$ meV Å^{-1} (1000 kV cm^{-1}) (broken line).

strong influence on the Raman spectrum of the confined phonon modes as will be discussed below.

III. PHONONS

We use the model originally introduced by Nusimovici and Birman[11] to calculate the bulk phonon dispersion in a wurtzite crystal. In this model the lattice potential is described by nearest-neighbor, next-nearest neighbor, and next-next-nearest neighbor restoring forces and terms associated with the distortion of bond angles and the long-range Coulomb interaction. The short-range part, V^{SR}, is given by

$$V^{\mathrm{SR}}=\sum_{1\mathrm{Ga\text{-}N}}\lambda_1(\delta r_{ij})^2+\sum_{2\mathrm{nd\ Ga\text{-}Ga}}\lambda_{2a}(\delta r_{ij})^2+\sum_{2\mathrm{nd\ N\text{-}N}}\lambda_{2b}(\delta r_{ij})^2+\sum_{3\mathrm{rd\ Ga\text{-}N}}\lambda_3(\delta r_{ij})^2+\sum_{\mathrm{N\text{-}Ga\text{-}N}}\lambda_{4a}(\delta\theta_{ijk})^2+\sum_{\mathrm{Ga\text{-}N\text{-}Ga}}\lambda_{4b}(\delta\theta_{ijk})^2.$$

δr_{ij} is the change in the distance between two atoms i and j from their equilibrium value and $\delta\theta_{ijk}$ is the change in the angle at the jth atom between the bonds joining the jth and ith atoms and the jth and kth atoms from their equilibrium value. The long-range Coulomb interaction is $V^C=\Sigma_{i,j}(q_iq_j/|\vec{r}_i-\vec{r}_j|)$, where the q_i are effective charges of the atom at the site $\vec{r}_i$ in the crystal with the constraint that the charges on Ga and N are of equal magnitude but with opposite sign so that the unit cell is charge neutral. So there is one free parameter, $q=|q_i|$, associated with the Coulomb interaction determining the difference in energies between transverse and longitudinal optical phonon frequencies.

The free parameters, the λ_i's, and the effective charge are found by fitting to the measured optical phonon frequencies.[9,6,8] The phonon modes, j, and their dispersion $\omega_j(\vec{q})$ are determined by diagonalizing a 12×12 dynamical matrix in the case of the wurtzite crystal symmetry since there are four atoms in the unit cell,[10]

$$\omega_j^2(\vec{q})w_k^{\alpha}(\vec{q},j)=\sum_{\beta,k'}D_{kk'}^{\alpha\beta}(\vec{q})w_{k'}^{\beta}(\vec{q},j), \tag{2}$$

where $\alpha,\beta=x,y,z$ and $\vec{w}_k(\vec{q},j)=\sqrt{M_k}\vec{u}_k(\vec{q},j)$. M_k is the mass of the kth atom in the unit cell and $\vec{u}_k(\vec{q},j)$ is its displacement in the jth mode at $\vec{q}$. The dynamical matrix, $D_{kk'}^{\alpha\beta}(\vec{q})$, is determined by second derivatives of V^{SR} and V^C with respect to the positions of the atoms and is block diagonal with four 3×3 matrices associated with displacements in the z direction and doubly degenerate modes in the x and y directions. Optical phonon frequencies have been measured by a number of groups for GaN (Refs. 6–8) and AlN.[6] However, there is only one published report on InN.[9] Here we use the most recent reported values. Along with frequencies of the modes measured in Raman experiments, the frequencies of the two B_1 modes are determined. These modes are Raman and infrared silent. The frequencies of these modes in wurtzite GaN, 315 cm^{-1} and 600 cm^{-1}, are similar to their values determined in hexagonal GaN.[7] Given these parameters the phonon dispersion curves, $\mathcal{E}_\nu(\vec{q})$, can be calculated and in particular those along the z direction, the direction of growth of the quantum wells, are shown in Fig. 3. The amount by which the curves disperse going from $q_z=0$ to $q_z=\pi/c$ determines the spread of confined phonon mode frequencies for each symmetry.

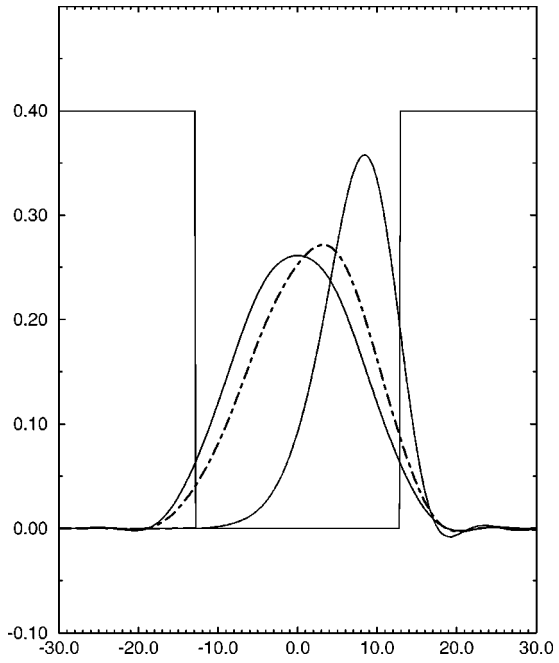

FIG. 2. Lowest confined hole subband in different electric fields, $E_0=0$ (solid line), $E_0=0.1$ meV Å^{-1} (100 kV cm^{-1}) (dot-dashed) and $E_0=10$ meV Å^{-1} (1000 kV cm^{-1}) (broken line).

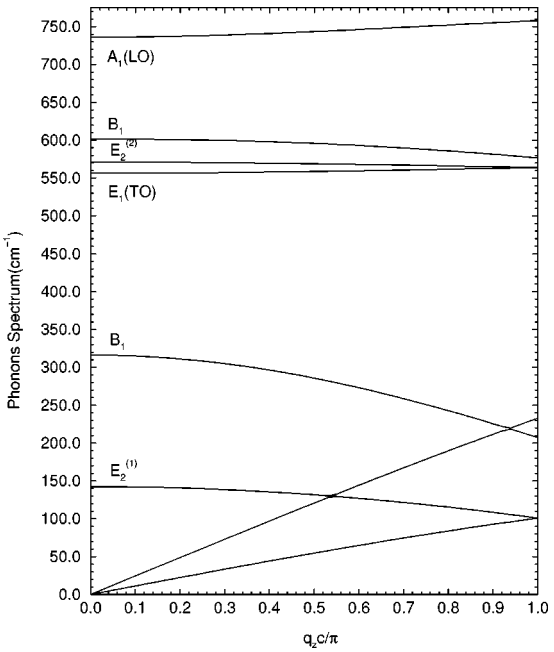

FIG. 3. Phonon spectrum for bulk GaN along the c axis calculated using the valence-Coulomb force field model. The different optical branches are labeled by the corresponding irreducible representation of the C_{6v}^4 space group.

Phonons of well material are given by $\phi_j(z) = e^{i\vec{q}\cdot\vec{\rho}}\sin(q_j^z z)$ for j even and $\phi_j(z) = e^{i\vec{q}\cdot\vec{\rho}}\cos(q_j^z z)$ for j odd, where $q_j^z = m\pi/(l_z+\Delta)$ for $j=1$ to n. n is the number of layers of the well material, so that $l_z = nc$, and Δ is the penetration of the confined phonon modes into the barrier material which is taken to one layer. The calculation of the Raman spectrum is carried out for the backscattering configuration and parallel polarizations for the incident and reflected beams. This probes the confined modes which correspond to bulk A_1(LO) symmetry. This mode has the greatest dispersion in the z direction, the direction of growth of the quantum well, and is about $\sim 20\ \mathrm{cm}^{-1}$ for GaN (see Fig. 3). In contrast, the E_1(TO) mode has a smaller dispersion across the zone, $\sim 5\ \mathrm{cm}^{-1}$, which would make it more difficult to resolve the corresponding confined phonon modes. The A_1(LO) confined modes have energies $\mathcal{E}_j = \omega(\vec{q}_{xy}=0, q_j^z)$ which, for $n=5$, can be resolved easily.

The absence of parity in the electronic states enhances the electron-phonon matrix elements for intrasubband scattering associated with the confined states.[13] In the next section the very strong influence on the Raman spectrum of this absence of parity will be discussed. For simplicity the confined modes are taken to have energies at $\mathcal{E}_{j=1} = 743\ \mathrm{cm}^{-1}$, $\mathcal{E}_{j=2} = 747\ \mathrm{cm}^{-1}$, $\mathcal{E}_{j=3} = 751\ \mathrm{cm}^{-1}$, $\mathcal{E}_{j=4} = 755\ \mathrm{cm}^{-1}$, and $\mathcal{E}_{j=5} = 759\ \mathrm{cm}^{-1}$.

IV. RAMAN CROSS SECTION

The Raman cross section is calculated using the interaction between the electromagnetic field and electron-hole pairs, H_{ER}, and the electron-phonon interaction, H_{EL}. H_{EL} can be thought of as coming from two contributions, H_{DF}, associated with deformation potentials, and H_{FR}, the Fröhlich interaction,

$$H_{\mathrm{ER}} = \sum_{\alpha}\left(\frac{-e}{m}\right)\sqrt{\frac{2\pi\hbar}{\Omega\eta_\alpha^2\omega_\alpha}}\hat{\epsilon}_\alpha\cdot\vec{p}\,e^{i\vec{k}_\alpha\cdot\vec{r}}\hat{a}_\alpha,$$

$$H_{\mathrm{EL}} = H_{\mathrm{EL}}^{\mathrm{DF}} + H_{\mathrm{EL}}^{\mathrm{FR}},$$

$$H_{\mathrm{EL}}^{\mathrm{DF}} = \sum_{q\nu}\sqrt{\frac{2\pi\hbar\Omega_c}{\Omega 2\mu a_0^2\mathcal{E}_{\vec{q}\nu}}}\int d\vec{r}D^{\nu}(\vec{r}) \times[e^{i\vec{q}_\nu\cdot\vec{r}}\hat{b}_\nu\hat{\psi}^\dagger(\vec{r})\hat{\psi}(\vec{r}) + \mathrm{H.c.}],$$

$$H_{\mathrm{EL}}^{\mathrm{FR}} = \sum_{q\nu}\int d\vec{r}\sqrt{\frac{2\pi e^2\mathcal{E}_{\vec{q}\nu}}{\Omega q^2}\left(\frac{1}{\epsilon_\infty}-\frac{1}{\epsilon_0}\right)} \times[ie^{i\vec{q}_\nu\cdot\vec{r}}\hat{b}_\nu\hat{\psi}^\dagger(\vec{r})\hat{\psi}(\vec{r}) + \mathrm{H.c.}]. \quad (3)$$

Ω is the volume of the crystal, η_α is the refractive index of the material evaluated at the frequency ω_α of the photon, ν is the phonon band index, and a_0 is a characteristic length of the lattice.

The rate at which incident photons are scattered is given by

$$W_{fi} = \frac{2\pi}{\hbar}\left|\sum_{\alpha\beta}\frac{\langle i|H_{\mathrm{ER}}|\alpha\rangle\langle\alpha|H_{\mathrm{EL}}|\beta\rangle\langle\beta|H_{\mathrm{ER}}|f\rangle}{(E_\alpha - E_l)(E_\alpha - E_l)}\right|^2 \times\delta(E_l - E_s - \mathcal{E}_{\vec{q}\nu}). \quad (4)$$

$|\alpha\rangle$ and $|\beta\rangle$ are excitonic states from the valence bands discussed above. $|i\rangle$ is the initial state with an incident photon of energy E_l and polarization $\hat{\epsilon}_l$. $|f\rangle$ is the final state with a scattered photon of energy E_s and polarization $\hat{\epsilon}_s$ and an additional phonon energy $\mathcal{E}_{\vec{q}\nu}$, where ν denotes the symmetry and LO or TO nature for polar phonons. The index α denotes the quantum numbers of the electron-hole pair. These include the total momentum of the pair, $\vec{K}$, the conduction band, c, and the valence band, v, from which the electron and hole come, and the internal exciton state, whether it is a bound state or a free Coulombic wave function. Using an envelope approximation for the wave function, $\Psi_{n_e,n_h,n_X}(z_e,z_h,\rho) = \phi_{n_e}(z_e)\psi_{n_h}(z_h)\Lambda_{n_X}(\rho)e^{i\vec{K}\cdot\vec{R}_{\mathrm{cm}}}$, so that $|\alpha\rangle = |n_e,n_h,\vec{K},n_X\rangle$, $\langle i|H_{\mathrm{ER}}|\alpha\rangle$ is given by

$$\langle i|H_{\mathrm{ER}}|\alpha\rangle = \left(\frac{-e}{m}\right)\sqrt{\frac{2\pi\hbar^2}{\Omega\eta_l^2 E_l}}\delta(\vec{k}_l - \vec{K})\Omega^{1/2}\Lambda_{n_X}(0) \times\langle\phi_{n_e}|\psi_{n_h}\rangle\langle c|\hat{\epsilon}_\alpha\cdot\vec{p}|v_\alpha\rangle. \quad (5)$$

There is a similar expression for $\langle f|H_{\mathrm{ER}}|\beta\rangle$ and W_{fi} becomes

$$W_{fi} = \frac{2\pi}{\hbar}\left|\frac{8\pi e^2}{\eta_l\eta_s\sqrt{E_l E_s}}\frac{\hbar^2}{2m}\frac{P^2}{2m} \times\sum_{\alpha,\beta}\frac{\Lambda_{n_X}(0)\Lambda_{n_X'}(0)}{(E_\alpha - E_l)(E_\beta - E_s)}\langle\phi_{n_e'}|\psi_{n_h'}\rangle\langle\phi_{n_e}|\psi_{n_h}\rangle \times\langle c|\hat{\epsilon}_l\cdot\vec{p}|v\rangle\langle c'|\hat{\epsilon}_l\cdot\vec{p}|v'\rangle\langle\alpha|H_{EL}|\beta\rangle\right|^2$$

$$\times \delta(E_l - E_s - \mathcal{E}_\lambda)\,\delta(\vec{k}_l - \vec{k}_s - \vec{q}), \tag{6}$$

where $|\beta\rangle = |n_e', n_h', \vec{K}', n_X'\rangle$, $\langle c|\hat{\epsilon}_l \cdot \vec{p}|v\rangle$, and $\langle c'|\hat{\epsilon}_l \cdot \vec{p}|v'\rangle$ are dimensionless matrix elements scaled by $P = 2\pi\hbar/a_0$ which is a characteristic magnitude for these matrix elements.

$\langle \alpha|H_{\rm EL}|\beta\rangle$ is given by the Fröhlich interaction in a quantum well,

$$\langle \alpha|H_{\rm EL}|\beta\rangle = \sum_{\vec{q}\,\nu} \sqrt{\frac{2\pi e^2 \mathcal{E}_{\vec{q}\,\nu}}{\Omega q^2}} \left(\frac{1}{\epsilon_\infty} - \frac{1}{\epsilon_0}\right) \times \left[\int dz\, \phi^*_{n_e}(z) F_j(z) \phi_{n_e'}(z)\, \delta_{n_h n_h'} - \int dz\, \psi^*_{n_h}(z) F_j(z) \psi_{n_h'}(z)\, \delta_{n_e n_e'}\right], \tag{7}$$

where $F_j(z)$ is the Fröhlich potential[17]

$$= e^{q_{xy} z}\left[e^{[q_{xy}(d+\Delta/2)]} - (-1)^j e^{-[q_{xy}(d+\Delta/2)]}\right], \quad z < -\frac{d+\Delta}{2},$$

$$F_j(z) = 2\cos q_z\left[z + \left(\frac{d+\Delta}{2}\right)\right] - e^{-[q_{xy}(d+\Delta/2))} \times \left[e^{-q_{xy} z} + (-1)^j e^{q_{xy} z}\right], \quad |z| \leqslant \frac{d+\Delta}{2}, \tag{8}$$

$$= e^{-q_{xy} z}\left[(-1)^j e^{q_{xy}(d+\Delta/2)} - e^{-q_{xy}(d+\Delta/2)}\right], \quad z > \frac{d+\Delta}{2}.$$

Here we consider the case of Raman spectra from experiments in the backscattering geometry. In the absence of an electric field across the well, the electronic states have even or odd parity and the Raman signal is dominated by the $j = 2$ and $j = 4$ confined phonons. In this case the $\langle \phi_{n_e}|\psi_{n_h}\rangle$ factors in $\langle i|H_{\rm ER}|\alpha\rangle$ and the parity of the $F_j(z)$'s ensure that W_{fi} is dominated by $n_e = n_e' = n_h = n_h' = 1$ and that it is small because of the near cancellation of the two integrals in the square brackets in Eq. (7).

As soon as an electric field is applied, the electron and hole subbands no longer have even and odd parity and the $\langle \phi_{n_e}|\psi_{n_h}\rangle$ factors no longer constrain the kinds of excitonic states which appear in the sum. As well as allowing for new contributions to $\langle \alpha|H_{\rm EL}|\beta\rangle$, large contributions appear where there is no longer substantial cancellation between the integrals in the square bracket of Eq. (7). These effects are shown in Figs. 4, 5, and 6, where the different confined phonon signals are modeled by Lorentzian line shapes with a half-width of 0.1 meV. In Fig. 4 the Raman spectrum for an electric field of 1 meV Å^{-1} is compared with the spectrum in the absence of a field. Even at this strength of field, which is relatively modest compared to the estimates of fields due to lattice mismatch given by Martin *et al.*,[22] the parity forbidden $j = 1$ and $j = 3$ confined phonons appear in the spectrum. When the electric fields are increased to values more characteristic of the lattice mismatch fields, 5meV Å^{-1} and 10 meV Å^{-1} (Fig. 5), the spectrum is dominated by these confined phonons and their intensity is strongly enhanced over that of the $j = 2$ and $j = 4$ phonons found in the absence

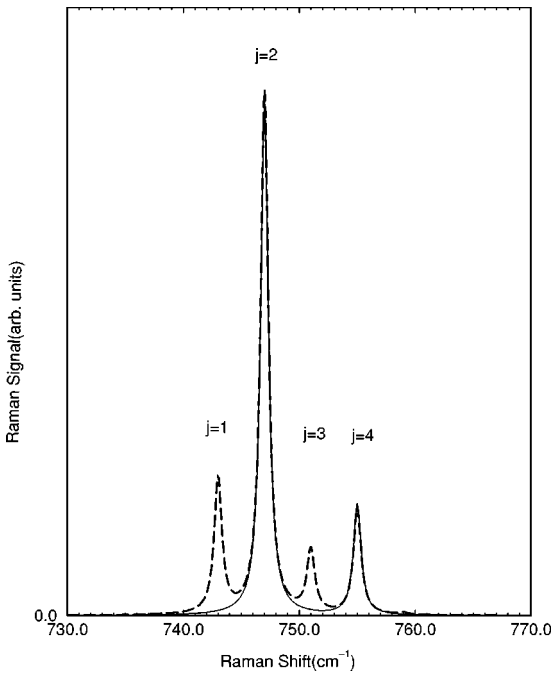

FIG. 4. Raman signal from the confined phonons in the absence of an electric field and with the additional features from the $j = 1$ and $j = 3$ phonons which arise with an electric field $E_0 = 1$ meV Å^{-1} (100 kV cm^{-1}) (dashed line). When $E_0 = 0$ only the $j = 2$ and $j = 4$ phonons are seen. When $E_0 = 1$ meV Å^{-1} (100 kV cm^{-1}) these modes gives the same strength signal but now there are also signals from the $j = 1$ and $j = 4$ modes because of the breakdown of the parity selection rule.

of internal electric fields. This is brought out further in Fig. 6, where it can be seen that the zero field $j = 2$ signal is smaller than either the $j = 1$, $j = 2$, or $j = 3$ phonons in large fields. The ''allowed'' $j = 4$ mode would be hard to resolve from the $j = 3$ in large fields because its contribution is suppressed compared to the zero field value and because the large $j = 3$ signal spreads out to the $j = 4$ mode energy even with a small width (0.1 meV). It can also be seen from Fig. 6 that at large fields the $j = 5$ confined phonon begins to contribute.

The striking feature of Figs. 4, 5, and 6 is the extent to which the results for an electric field of 10 meV Å^{-1} resemble the results in the absence of an electric field in that both spectra are dominated by one peak. However, in the case of $E_0 = 0$, the peak is for the $j = 2$ confined phonon whereas in the $E_0 = 10$ meV Å^{-1} case the peak is the $j = 1$ confined phonon. It is clearly important to take into account these potentially large electric fields in interpreting the Raman data if the phonons are to be identified correctly.

Raman spectra in applied electric fields have been studied before in $Al_xGa_{1-x}As$-GaAs heterostructures and their influence on the Raman signal from confined phonons was investigated.[15,17] The electric field strengths in these experiments were comparable to the intrinsic fields expected in the nitride heterostructures due to lattice mismatch. This suggests that the application of an external electric field could modulate significantly the intrinsic fields and would provide a useful probe of their strength. In the case of an undoped quantum well the magnitude of these intrinsic electric fields can be determined by the application of an external field so

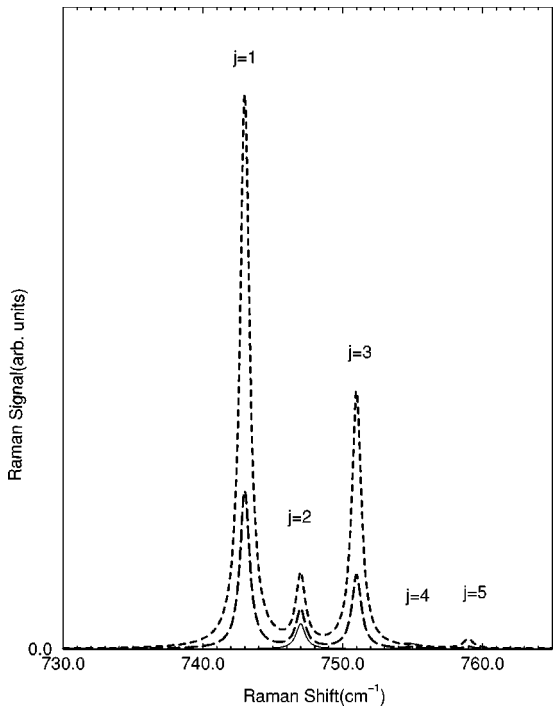

FIG. 5. Raman signal from the confined phonons in different electric fields, $E_0=0$ (solid line), $E_0=5$ meV Å^{-1} (500 kV cm^{-1}) (long-dashed), and $E_0=10$ meV Å^{-1} (1000 kV cm^{-1}) (short-dashed). When $E_0=0$ only the $j=2$ and $j=4$ phonons are seen. The Raman signal is completely dominated by the $j=1$ and $j=3$ phonons in the $E_0=5$ meV Å^{-1} (500 kV cm^{-1}) and $E_0=10$ meV Å^{-1} (1000 kV cm^{-1}) fields.

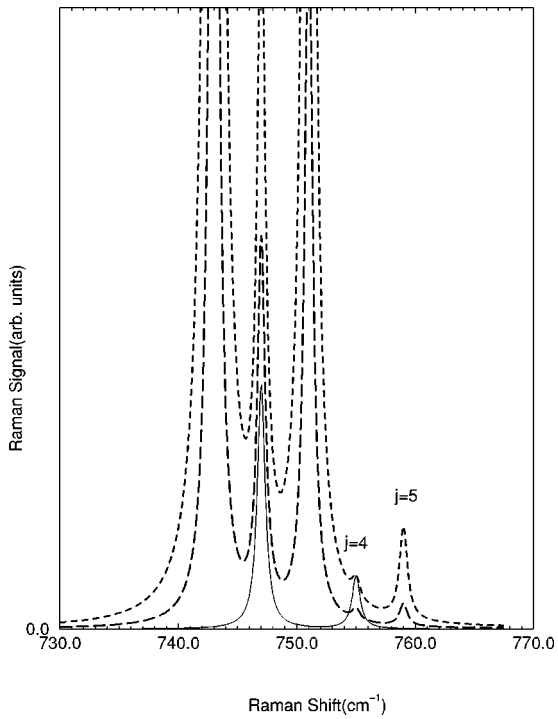

FIG. 6. A comparison of the $E_0=0$ signal with the $E_0=5$ meV Å^{-1} (500 kV cm^{-1}) (long-dashed) and $E_0=10$ meV Å^{-1} (1000 kV cm^{-1}) (short-dashed) fields. The $j=2$ signal with $E_0=0$ is smaller than the $j=1$,$j=2$, or $j=3$ with $E_0=5$ meV Å^{-1} (500 kV cm^{-1}) and $E_0=10$ meV Å^{-1} (1000 kV cm^{-1}). Application of strong fields suppresses the $j=4$ signal so that it is hard to resolve from the $j=3$ signal.

that the net field in the well is zero, which is signaled by the appearance of only the parity allowed confined phonons in the Raman spectrum.

By sweeping the laser frequency, E_l, and monitoring the scattered radiation at an energy $E_s=E_l-\mathcal{E}_\lambda$, where $\mathcal{E}_\lambda$ is the energy of the $j=2$ confined A_1(LO) phonon, the contributions from the different subbands are seen. When one does this, the importance of including subbands of different parity for calculating strength of the signal in a field becomes evident. Resonant Raman experiments would pick these contributions and would provide a useful test of the subband structure.

V. CONCLUSION

We have shown that intrinsic electric fields present in wurtzite heterostructures can have a strong influence on the Raman spectrum and that an analysis of the Raman spectrum which does not include the breakdown of parity selection rules caused by these fields would lead to an incorrect identification of the phonon modes. This breakdown is a measure of the electric fields present in the heterostructures which come from lattice mismatch and spontaneous polarization. Given a model for heterostructure phonon modes, an analysis of the Raman spectrum data can provide an estimate of the strain and the extent to which the strain has been relaxed by defect formation. The strong dependence of the Raman spectrum on electric field suggests that external electric fields are a useful probe of nitride heterostructures.

ACKNOWLEDGMENT

This work was supported by the Army Research Office under the auspices of the U.S. Army Research Office Scientific Services Program administered by Battelle.

[1] B. C. Lee, K. W. Kim, M. Dutta, and M. A. Stroscio, Phys. Rev. B **56**, 997 (1997).

[2] F. Bernardini, V. Fiorentini, and D. Vanderbilt, Phys. Rev. Lett. **79**, 3958 (1997).

[3] F. Bernardini, V. Fiorentini, and D. Vanderbilt, Phys. Rev. B **56**, R10 024 (1997).

[4] F. Bernardini and V. Fiorentini, cond-mat/9803384 (unpublished).

[5] B. Tell, T. C. Damen, and S. P. S. Porto, Phys. Rev. **144**, 771 (1966); C. A Arguello, D. L. Rousseau, and S. P. S. Porto, *ibid.* **181**, 1351 (1969).

[6] *Properties of Group III Nitrides*, edited by J. H. Edgar (Inspec, London, 1988), Chap. 8.

[7] H. Siegle, L. Filippidis, C. Kaczmarczyk, A. P. Litvinchuk, A. Hoffman, and C. Thomsen, *23rd International Conference on The Physics of Semiconductors*, edited by M. Scheffler and R.

Zimmerman (World Scientific, Singapore, 1996), Vol. 1, p. 539.
[8] J. M. Zhang, T. Ruf, M. Cardona, O. Ambacher, M. Stutzman, J. M. Wagner, and F. Bechstedt, Phys. Rev. B **56**, 14 399 (1997).
[9] H.-J. Kwon, Y.-H. Lee, O. Miki, H. Yamano, and A. Yoshida, Appl. Phys. Lett. **69**, 937 (1996).
[10] M. Born and K. Huang, *Dynamical Theory of Crystal Lattices* (Clarendon Press, Oxford, England, 1954).
[11] M. A. Nusimovici, M. Balkanski, and J. L. Birman, Phys. Rev. **156**, 925 (1967); Phys. Rev. B **1**, 595 (1970).
[12] G. Kanellis, J. F. Morhange, and M. Balkanski, Phys. Rev. B **28**, 3390 (1983); **28**, 3398 (1983); **28**, 3406 (1983).
[13] S. Das Sarma, V. B. Campos, M. A. Stroscio, and K. W. Kim, Semicond. Sci. Technol. **7**, 60 (1992).
[14] A. K. Sood, J. Menéndez, M. Cardona, and K. Ploog, Phys. Rev. Lett. **54**, 2115 (1985).
[15] T. Suemoto, G. Fasol, and K. Ploog, Phys. Rev. B **34**, 6034 (1986).
[16] H. Tang, B. Zhu, and K. Huang, Phys. Rev. B **42**, 3082 (1990).
[17] A. J. Shields, C. Trallero-Giner, M. Cardona, H. T. Grahn, K. Ploog, V. A. Hailer, D. A. Tenney, N. T. Moshegov, and A. I. Toropov, Phys. Rev. B **46**, 6990 (1992).
[18] T. L. Tansley and R. J. Egan, Phys. Rev. B **45**, 10 942 (1992).
[19] M. Suzuki, T. Uenoyama, and A. Yanase, Phys. Rev. B **52**, 8132 (1995).
[20] J.-B. Jeon, Yu. M Sirenko, K. W. Kim, M. A. Littlejohn, and M. A. Stroscio, Solid State Commun. **99**, 423 (1996).
[21] K. Kim, W. R. L. Lambrecht, B. Segall, and M. van Schilfgaarde, Phys. Rev. B **56**, 7363 (1997).
[22] G. Martin, A. Botchkarev, A. Rockett, and H. Morkoc, Appl. Phys. Lett. **68**, 2541 (1996).
[23] Z. Sitar, M. J. Paisley, B. Yan, J. Ruan, W. J. Choyke, and R. F. Davis, J. Vac. Sci. Technol. B **8**, 316 (1990).
[24] M. Shinada and S. Sugano, J. Phys. Soc. Jpn. **21**, 1936 (1966).